ACS OMEGA

Article

Cite This: ACS Omega 2018, 3, 16777−16783

http://pubs.acs.org/journal/acsodf

Mimicking the Secretory Action of a Gland by a Composite System Made of a pH-Responsive Surfactant-Based Hydrogel and a Dialysis Membrane

Alessio Cesaretti,[†] Irene Di Guida,[†] Naishka E. Caldero-Rodríguez,[†,‡] Catia Clementi,[†] Raimondo Germani,[†] and Pier Luigi Gentili*[,†]

[†]Department of Chemistry, Biology and Biotechnology, University of Perugia, Via Elce di sotto 8, Perugia 06123, Italy

[‡]Department of Chemistry, College of Natural Sciences, University of Puerto Rico, Río Piedras Campus, San Juan 00931-3346, Puerto Rico

Supporting Information

ABSTRACT: The hydrogel obtained by a zwitterionic N-oxide surfactant is proposed as the core of a pH-responsive artificial gland model. The viscosity and pH variations, induced by pulse additions of acid and base, are investigated by a pyridinium salt and alizarin red S, respectively. The artificial gland model is implemented by enclosing the gel within a dialysis membrane, and its secretory action is tested by monitoring the release of a fluorescent acridinium salt.

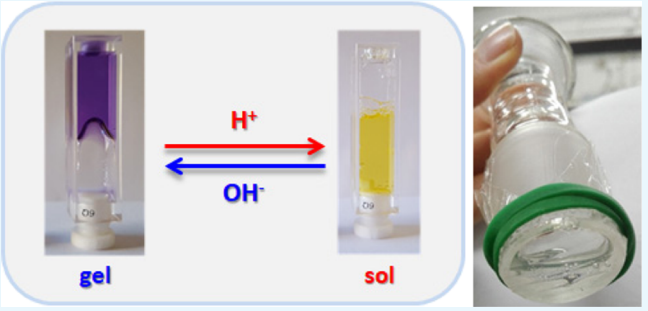

INTRODUCTION

The technological development of our society is guided by the will of helping humans in manual and mental labor. With the advent of the industrial revolution, which began in the 18th century, many machines performing heavy manual labor have been devised, thus leading to noticeable economic and social progress. Since the early 1950s, electronic computers instructed by software have been contrived to perform numerical computations and relieve humans from mental labor. A long-cherished aspiration is to design machines that can help humans in both manual and mental activities at the same time. Such machines, called robots, are programmable and potentially able to carry out many actions peculiar to humans.[1] In fact, robots are usually able to perceive signals through sensors, plan actions through internal cognitive processes, and act through actuators, like the human nervous system does through its sensory cells, brain, and effector system made of muscles and glands. Traditionally, robots are made of electronic circuits, computer software, mechanical rigid parts, and electric motors and are designed especially for accomplishing dangerous tasks, such as bomb disposal and deep ocean and planetary exploration. Recently, the idea of developing robots grounded on wetware rather than on hardware is taking shape.[2−11] A "soft robot", also called "chemical robot", is thought as a molecular assembly that reacts autonomously to its environment through molecular sensors, makes decisions by its intrinsic artificial neural networks, and performs actions upon its environment through molecular effectors. Chemical robots should be easily miniaturized and implanted in living beings to interplay with cells or organelles for biomedical applications.

After proposing molecular sensors[12−14] and artificial neural models,[15−17] in this work, we present a surfactant-based hydrogel, combined with a dialysis membrane (**DM**), as a pH-sensitive secreting gland model. In the human effector system, glands are sac-like tissue structures, which play vital roles in the physiology of many organs by secreting either hormones or fluids. Glands exert their secretory action in response to excitatory inputs coming from the brain; these inputs can be either periodic or occasional. We show that it is possible to mimic the secretory action of a gland by using the pH-sensitive gel generated by the amphoteric *p*-dodecyloxybenzyldimethylamine N-oxide (**pDoAO**) surfactant (see Chart 1) as the core and a **DM** as the boundary. The composite system is indicated as **pDoAO** + **DM**, hereinafter. On the one hand, an acidic input promotes the gel-to-sol transition; on the other hand, a basic input restores the gel state. We use the fluorescent *N*-octyl-acridinium perchlorate ($\mathbf{C_8Ac}$) as a hormone-like compound for the **pDoAO** + **DM** artificial gland model. To monitor the pH-induced gel−sol transitions and the properties of the gel and sol phases of **pDoAO**, we have chosen two compounds as follows: alizarin red S (**ARS**) as the pH probe and 2,4-(diphenylamino)phenyl-ethenyl-1-methylpyridinium iodide (**PyI**) as the viscosity probe (Chart 1).

Received: October 25, 2018
Accepted: November 26, 2018
Published: December 6, 2018

DOI: 10.1021/acsomega.8b02940
ACS Omega 2018, 3, 16777−16783

Chart 1. Molecular structures of the zwitterionic surfactant pDoAO, the probes ARS and the pyridinium salt (PyI), and the acridinium salt (C_8Ac)

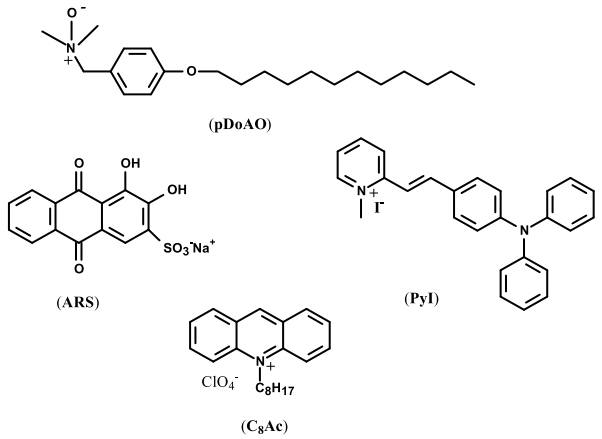

RESULTS AND DISCUSSION

The amphoteric **pDoAO** surfactant has pK_a = 4.9 in water.[18] When the pH of the solution is neutral or alkaline, the **pDoAO** molecules are zwitterionic and they carry no net charges. Under these conditions, previous structural investigations[18,19] revealed that when the concentration of **pDoAO** is larger than the critical micellar value (cmc = 1.6 × 10^{-5} M), **pDoAO** molecules spontaneously self-assemble into long, flexible wormlike micelles that are interconnected in dynamic network structures because of the weak repulsion between the neutral headgroups and the adhesive action of the hydrocarbon tails. At acidic pH < pK_a, the single **pDoAO** molecules become positively charged, thus affecting the supramolecular structure of the micelles. In fact, it has been shown[18,19] that the wormlike micelles become shorter and their networks become less entangled and viscous.

The **ARS** salt is a dye whose UV−visible absorption spectrum depends appreciably on the pH of the solution (see Figure 1A). The two hydroxyl groups (see Chart 1) have two distinct pK_{ai} values, which are 5.5 (pK_{a1}) and 11 (pK_{a2}), respectively.[20] At pH ≈ 3, **ARS** is in its monoanionic form (see Chart 1) and its absorption spectrum, in the visible region, is characterized just by one band centered at 421 nm, conferring a yellow color to its solution. At pH ≈ 7.5, **ARS** is mainly in its dianionic form and its absorption spectrum in the visible region consists of a broad band centered at 495 nm, conferring a magenta color. In Milli-Q water, at pH ≈ 5.5, the **ARS** spectrum is a convolution of the contribution of the bands at 421 and 495 nm because its solution contains a mixture of the mono- and dianionic forms. When **ARS** is dissolved in water, buffered at pH = 7.5, at a concentration of 8.0 × 10^{-5} M and in the presence of **pDoAO** micelles, in a ratio [micelles]/[**ARS**] ≈ 15, the characteristic band of dianionic **ARS** is red-shifted from 495 to 540 nm (giving a purple color) and it is slightly less intense (see the last spectrum in Figure 1B showing the titration of **ARS** with **pDoAO**; Table S1 in the Supporting Information contains the details of the additions). This spectral modification suggests that the dianionic **ARS** molecules interplay with the micellar aggregates, which have the surfactants in their zwitterionic state, and the equilibrium association constant has been estimated to be K = 550 (see eq. S1 and Figure S1 in the Supporting Information). When **ARS** is dissolved in water, buffered at pH = 3.1, at a concentration

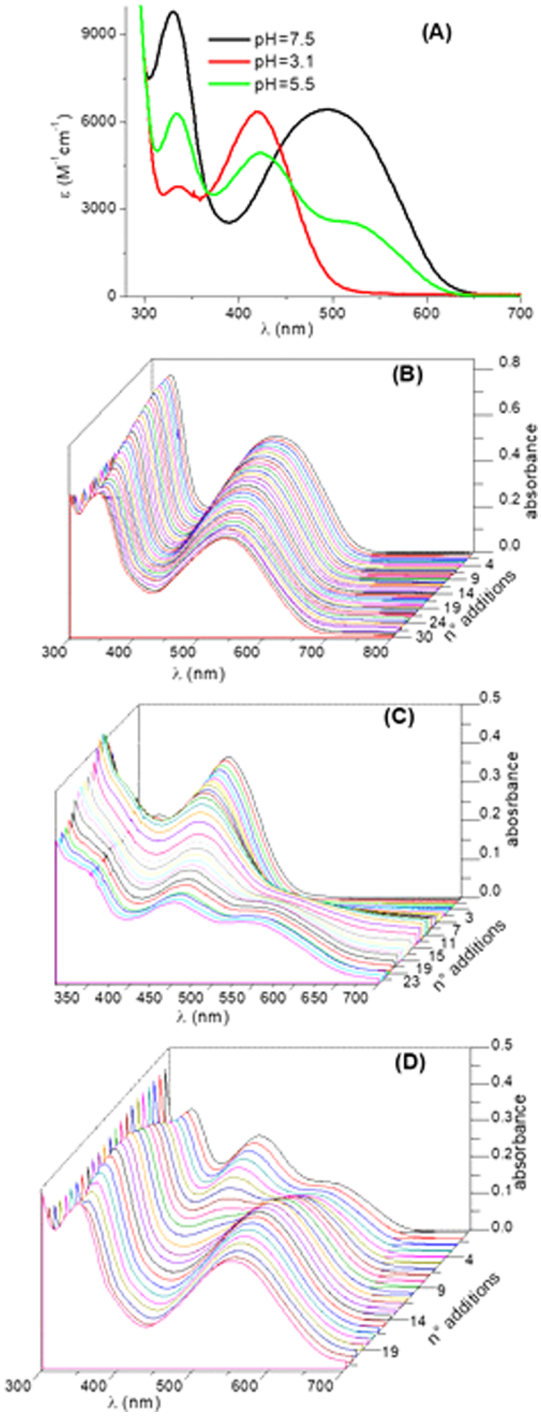

Figure 1. Absorption spectra of **ARS** in water at different pHs in (A); titration of **ARS** with **pDoAO** at pH = 7.5 in (B), at pH = 3.1 in (C), and in pure water in (D). The plotted spectra have been corrected by considering the dilution due to each addition of the surfactant solution. The values of the ratio [**pDoAO**]/[**ARS**], at every addition, are reported in the Supporting Information.

of 5.8 × 10^{-5} M and in the presence of **pDoAO** micelles, in a ratio [micelles]/[**ARS**] ≈ 11, the band of the monoanionic form red-shifts and wanes in favor of the appearance of a spectral contribution in the region of dianionic **ARS** (see the last spectrum in Figure 1C showing the titration of **ARS** with **pDoAO**; Table S2 contains the details of the additions). The spectral evolution in Figure 1C reveals that the monoanionic

DOI: 10.1021/acsomega.8b02940
ACS Omega 2018, 3, 16777−16783

ARS molecules interplay with the micelles, consisting of both protonated and zwitterionic surfactants, and they are presumably shielded by the micelles, wherein they partially deprotonate. The association constant between **ARS** and the micelles has been estimated to be K = 4700 (see Figure S2). When **ARS** is dissolved in pure unbuffered water at 5.4×10^{-5} M and in the presence of **pDoAO** micelles, in a ratio [micelles]/[**ARS**] ≈ 9, the band of the monoanionic form, at 421 nm, wanes in favor of the red-shifted band of the dianionic form, at 540 nm (see the last spectrum in Figure 1D showing the titration of **ARS** with **pDoAO**; Table S3 contains the details of the additions). This spectral evidence confirms that the zwitterionic **pDoAO** surfactants deprotonate the monoanionic **ARS** and the resulting dianionic **ARS** molecules interplay with the micelles through an equilibrium association constant K = 4600 close to that estimated at pH = 3.1 (see Figure S3).

When the concentration of **pDoAO** in pure water is increased from ≈5×10^{-4} to 7×10^{-3} M, the solution zero-shear viscosity rises more than 10 times, from $\eta \approx 1$ cP up to $\eta \approx 11$ cP. The increase in [**pDoAO**] makes the network of wormlike micelles so entangled that the solution becomes viscoelastic.[18] When [**pDoAO**] ≈10^{-1} M, the system becomes a firm gel, having $\eta \approx 2900$ cP. It is possible to probe this viscosity growth by using the push-pull **PyI** compound (see Chart 1). **PyI** is both a polarity and a viscosity probe because of its mechanism of relaxation after photoexcitation. Its relaxation pathway involves a first fluorescent Franck-Condon excited state, which can relax to a structural twisted charge-transfer state emitting at lower energies.[21] The polarity of the microenvironment affects the shape, position, and intensity of **PyI** fluorescence emission,[21] whereas the viscosity mainly affects intensity. In fact, the stronger the viscosity, the higher the **PyI** fluorescence quantum yield, and a linear relation between Φ_F(**PyI**) and log(η) has been found (see the data in Figure S4). The tighter the **pDoAO** micelle web, the more hindered the **PyI** structural rearrangement and the higher the probability of **PyI** emission. The viscosities of both the viscoelastic solution (when [**pDoAO**] ≈ 10^{-2} M) and the gel (when [**pDoAO**] ≈ 10^{-1} M) are pH-sensitive. Figure 2 shows the effect of consecutive injections of acid and base in a viscoelastic **pDoAO** solution (see also Figure S5 in Supporting Information, for the analytical details of the single injections). Before any addition, the system is characterized by the following parameters: pH ≈ 7, Φ_F(**PyI**) ≈ 0.035, and $\eta \approx 11$ cP. After the first addition of acid, both pH and Φ_F(**PyI**) as well as η decrease appreciably. The addition of acid protonates the oxygen atoms of the N^+-O^- groups, and the surfactant molecules, becoming positively charged, repel mutually. The ultimate micro-heterogeneous effect of acid addition is a shattered web of small rodlike micelles (according to the previous structural investigations[18,19]), exhibiting a reduced viscosity with respect to that of the original entangled web. After neutralizing the acid by injection of an equimolar amount of NaOH, both pH and Φ_F(**PyI**) as well as η jump well beyond the initial values, recorded before any addition of acid and base. The high pH (≈ 11), achieved by the addition of NaOH, guarantees the deprotonation of all of the N^+-OH groups, which become zwitterionic. The threads of wormlike micelles can self-assemble tightly without suffering electrostatic repulsions. The resulting network shows the highest Φ_F(**PyI**) (≈0.09) and the strongest viscosity ($\eta \approx 620$ cP). Further sequential injections of acid and base reproduce the consecutive drop and growth of pH, Φ_F(**PyI**), and η. However, the extent of the pH, Φ_F(**PyI**), and η variations [ΔpH, $\Delta\Phi_F$(**PyI**), and Δ(log(η))] tends to shrink monotonically in the first consecutive injections. After eight additions of acid and base, ΔpH, $\Delta\Phi_F$(**PyI**), and Δ(log(η)) stabilize to 5, 0.04, and 1.2, respectively, except for random fluctuations. The initial shrinking of ΔpH, $\Delta\Phi_F$(**PyI**), and Δ(log(η)) is ascribable to a sort of ageing effect in the acidified solution of **pDoAO**. This ageing effect is reproducible and detectable even by injecting amounts of acid and base different from those used to obtain the results shown in Figure 2 (see, for instance, Figure S6). Of course, the extent of ΔpH, $\Delta\Phi_F$(**PyI**), and Δ(log(η)) depends on how much acid and base is added every time. They are maximized when acid and base are added in excess with respect to the moles of **pDoAO**. Moreover, the shrinking of ΔpH, $\Delta\Phi_F$(**PyI**), and Δ(log(η)) is particularly pronounced if the anion of the acid interplays strongly with the N^+-OH, for example, if the acid is HCl (see Figure S7). The cause of the ageing effect is the accumulation of ionic salts (such as Na^+HCOO^- or Na^+Cl^-) in the solution of cationic surfactant molecules, which screens repulsive electrostatic interaction and induces the formation of a network of threadlike micelles accompanied by viscosity increase.[18]

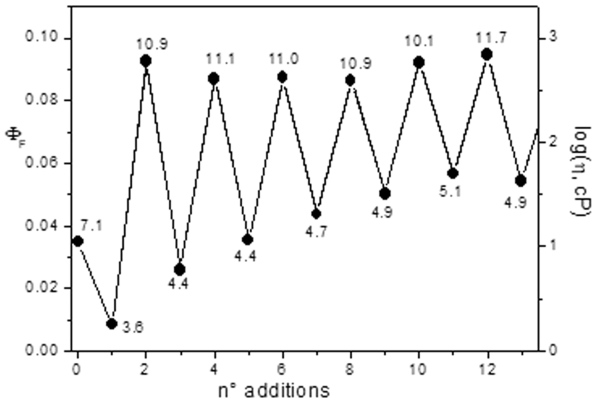

Figure 2. Effect of acid (HCOOH) and base (NaOH) additions on Φ_F of **PyI** (2×10^{-5} M) and the logarithm of viscosities (η in cP) of the viscoelastic solutions containing [**pDoAO**] ≈ 10^{-2} M. The values close to the dots in the graph correspond to the pH of the solution after every addition.

When [**pDoAO**] ≈ 10^{-1} M, the solution is a gel with pH ≥ 7 and $\eta \approx 2900$ cP. The pH of the gel is probed by **ARS** whose spectrum (see Figure 3C) exhibits the characteristic band of the dianionic form embedded within the **pDoAO** micelle network (the maximum of the absorption band is at 565 nm) and looks purple. The viscosity of the gel is probed by **PyI**, whose Φ_F is 0.17. By adding an equimolar amount of CH_3SO_3H, the pH and the viscosity drop. In fact, the system becomes an acidified sol. The acidity is probed by **ARS** whose absorption spectrum shows the characteristic band of the monoanionic form, centered at 434 nm, giving a yellow color. The reduction in viscosity is visible by naked eye (see Figure 3A,B) and is quantitatively monitored through the fluorescence quantum yield of **PyI**, which is equal to 0.13 and corresponds to $\eta \approx 510$ cP, that is, almost six times lower than the viscosity of the initial gel. By neutralizing the acid, the pH jumps to alkaline values, as confirmed by the absorption spectrum of **ARS**, which red-shifts and confers a purple color to the system (see Figure 3C,D). Moreover, the solution again becomes a

DOI: 10.1021/acsomega.8b02940
ACS Omega 2018, 3, 16777−16783

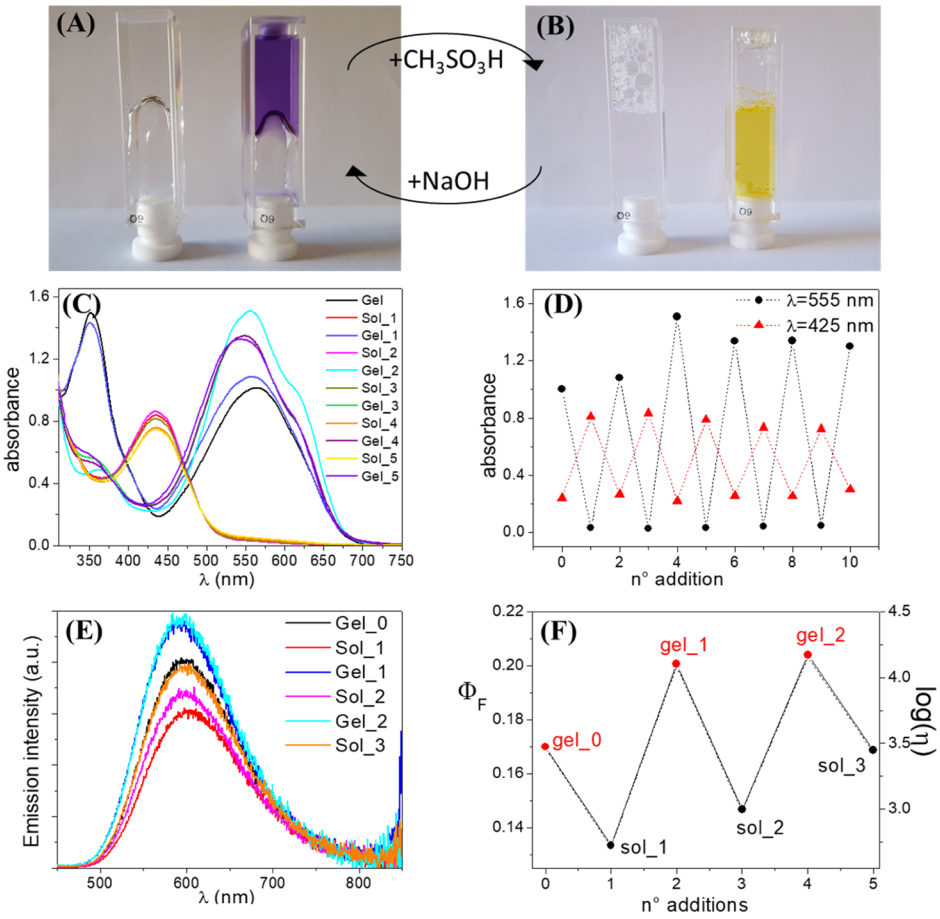

Figure 3. Gel (in A) to sol (in B) and reverse transition induced by the addition of CH_3SO_3H and NaOH, respectively, in the absence (left cuvette) and presence (right cuvette) of **ARS**. Spectral modification of **ARS** (in C,D) after the sequential injections of CH_3SO_3H and NaOH. Intensity changes in the emission spectrum of **PyI** (in E) and changes in Φ_F(**PyI**) and log(η) of the solution containing [**pDoAO**] $\approx 10^{-1}$ M (in F) due to sequential injections of equimolar amounts of CH_3SO_3H and NaOH.

gel, but with a much stronger viscosity: $\eta \approx 12\,200$ cP, as probed by Φ_F(**PyI**) that becomes 0.20 (see Figure 3E,F). This high viscosity is due to the surfactant molecules, which are now all in their zwitterionic form and show a very rigid network of entangled wormlike micelles. The probes, **ARS** and **PyI**, are in such small concentrations with respect to that of **pDoAO** that they do not affect the properties of the sol and gel phases. By injecting cyclically and repeatedly the acid and the base, the system with [**pDoAO**] $\approx 10^{-1}$ M shows an ageing effect similar to that found in the case of viscoelastic solutions with [**pDoAO**] $\approx 10^{-2}$ M (see Figure 3F). After the shrinking stage, the viscosity change associated with the gel−sol transition stabilizes and its excursion ranges between ≈14 000 cP (gel state) and ≈2700 cP (sol state), as probed by Φ_F(**PyI**) that varies from ≈0.20 to ≈0.17. The η values are 2 orders of magnitude larger than those spanned by the viscoelastic fluid shown in Figure 2, where the viscosity ranges between ≈690 and ≈40 cP, as soon as the ageing stage is completed.

The pH responsiveness of the zwitterionic **pDoAO**-based gel that has been presented in this work can be thus exploited to mimic the secretory action of a gland. The gel is segregated from a collecting aqueous solution through a **DM**. Figure 4 shows pictures of the device. The activity of the artificial gland model (**pDoAO** + **DM**) is tested by monitoring the secretion of the fluorescent probe **C_8Ac** that interplays with **pDoAO** through its positive charge and its long alkyl chain. The release

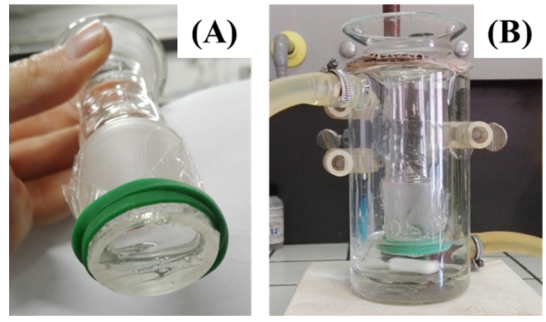

Figure 4. Structure of the artificial gland model. A glass tube closed at the bottom by the **DM** (A) and segregating the solution of the surfactant in water. The bottom part of the glass tube is immersed in water that is thermostated and under stirring within a beaker (B).

of **pDoAO** molecules is also monitored at regular time intervals (see the Experimental Section and paragraph I.3 of the Supporting Information for the details).

The results are shown in Figure 5. Figure 5A reports the molar fraction of **C_8Ac** secreted by the gel (squared red points) and the sol (circled black points) over time (determined fluorometrically). There is a significant difference between the two phases because in the case of the gel, the trend of $\chi_{(C_8Ac)}$ versus time reaches a plateau at 0.030 ± 0.005, whereas in the case of the sol, it grows monotonically up to a complete

DOI: 10.1021/acsomega.8b02940
ACS Omega 2018, 3, 16777−16783

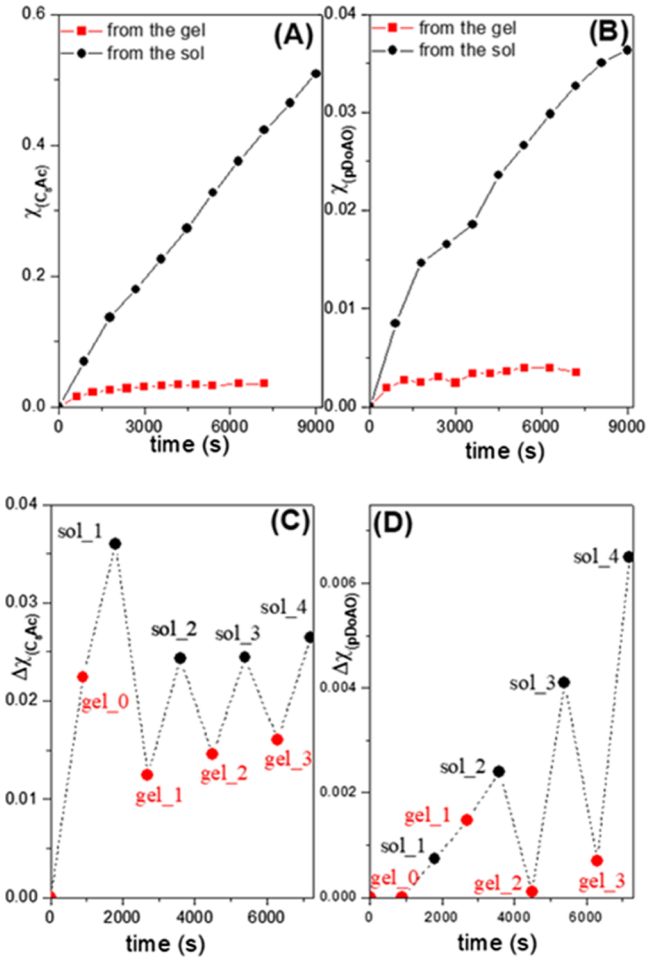

Figure 5. Trends of $\chi_{(C_8Ac)}$ (in A) and $\chi_{(pDoAO)}$ (in B) released over time by the artificial gland model (**pDoAO + DM**) in the gel (red squares) and sol (black circles) states, respectively. Trends of the molar fraction increments $\Delta\chi_{(C_8Ac)}$ (in C) and $\Delta\chi_{(pDoAO)}$ (in D) secreted by **pDoAO + DM** after sequential injections of CH_3SO_3H and NaOH, respectively. For the concentrations used, see the Supporting Information.

secretion of **C_8Ac** ($\chi_{(C_8Ac)} = 1.0 \pm 0.1$) in about 13 h. The different secretory activities of **pDoAO + DM** in its sol and gel states are due not only to the distinct viscosities of the two phases but also to the contribution of **DM**. In fact, as shown in paragraph I.4 of the Supporting Information, **DM** releases **C_8Ac** more easily from an acidic than from an alkaline aqueous solution. Figure 5B shows the release of the surfactant over time (determined spectrophotometrically). The behavior of the two phases is sharply different. From the gel phase, only $\chi_{(pDoAO)} = 0.0025 \pm 0.0005$ is lost in 2 h, and after reaching the plateau, $\chi_{(pDoAO)}$ does not grow over time. From the sol phase, a molar fraction of $\chi_{(pDoAO)} = (0.036 \pm 0.010)$ is released in 2 h, but it does not stop when the collecting solution is pure water. The composite system **pDoAO + DM** can be a promising artificial gland model if it also responds to periodic inputs. By injecting equimolar amounts of CH_3SO_3H and NaOH every 15 min (see the Supporting Information for the details), **pDoAO + DM** switches reversibly from the gel to the sol phase and back. Figure 5C shows the consecutive increments of $\chi_{(C_8Ac)}$ ($\Delta\chi_{(C_8Ac)}$) in the collecting aqueous solution. Figure 5D shows those of $\chi_{(pDoAO)}$ ($\Delta\chi_{(pDoAO)}$). The trend of Figure 5C confirms that the secretory power of the sol state is always larger than that of the gel state. Moreover, after the first injections of CH_3SO_3H and NaOH, **pDoAO + DM** exhibits an ageing effect analogous to that reported in Figure 3F. In fact, the viscosities of both the gel and the sol phases increase and the amounts of secreted **C_8Ac** decrease. Finally, Figure 5D confirms that the release of the surfactant is limited in the case of the gel state, whereas it is relentless in the case of the sol phase.

CONCLUSIONS

The composite **pDoAO + DM** system can play as a pH-responsive gland model releasing positively charged and relatively small molecules, such as **C_8Ac**. Because **pDoAO + DM** loses portions of its surfactant molecules as well, it can be an artificial model of an apocrine gland that has the peculiarity of releasing part of its cytoplasm in its secretions. To the best of our knowledge, our composite **pDoAO + DM** system is the first example of an artificial apocrine gland model devised through nonbiological systems. Its core, made of **pDoAO**, offers, as other previously investigated hydrogels based on smart wormlike micelles,[22] two advantages over alternative pH-responsive polymer gels:[23−25] first, the instantaneous response to ΔpH inputs and second, biocompatibility.[26,27] The **pDoAO** hydrogel also exhibits a peculiar ageing phenomenon that can be exploited as a memory effect, which is an added value for smart materials. To extend the secretory capabilities of our artificial gland model, we are scrutinizing the permeability of other membranes. Finally, **pDoAO + DM** can be transformed into an autonomous, chemically powered, pH-sensitive artificial gland model if it is integrated with a proper pH oscillatory chemical reaction.

EXPERIMENTAL SECTION

Materials. The zwitterionic surfactant **pDoAO** was synthesized according to the procedure described in ref 28. **ARS**, which is the sodium salt of 9,10-dihydro-3,4-dihydroxy-9,10-dioxo-2-antracenesulfonic acid (**ARS**) of analytic grade, was purchased from Carlo Erba and used without any further purification. The viscosity probe, 2,4-(diphenylamino)phenyl-ethenyl-1-methylpyridinium iodide (**PyI**), was synthesized according to the procedure described in ref 21. The probe **C_8Ac** was synthesized by quaternization of acridine with octyl-iodide in acetonitrile; then, the perchlorate anion was introduced by ionic exchange with sodium perchlorate in methanol.[29] To implement the artificial gland, the hydrogel made of **pDoAO** was embedded within a **DM**, 0.03 mm thick, made of cellulose with pores having an average diameter of 24 Å. The thickness of the membrane was 0.3 mm. The pH values of aqueous solutions at 3.1 and 7.5 were attained by Britton buffers prepared by mixing an acid solution (H_3BO_3 0.04 M, H_3PO_4 0.04 M and CH_3COOH 0.04 M) with a 0.2 M solution of NaOH, adjusting the ionic strength of the final solution at 5 mM.

Spectrophotometric Measurements. Steady-state absorption and emission spectra were recorded by using a PerkinElmer Lambda 800 spectrophotometer and a Horiba FluoroMax-4 spectrofluorimeter of HORIBA Scientific operated by FluorEssence, respectively. The latter gives back fluorescence emission spectra considering corrections for both the monochromator response and the detector sensitivity. Fluorescence quantum yields (experimental error of ca. 7%)

DOI: 10.1021/acsomega.8b02940
ACS Omega 2018, 3, 16777−16783

were determined from the emission spectra of samples whose absorbance at the excitation wavelength was lower than 0.1. The absorbance was maintained smaller than 0.1 to have a linear relationship between the absorbance and the emission intensity and avoid self-absorption effects. Tetracene (Φ_F = 0.16 in air-equilibrated cyclohexane)[30] was used as the fluorometric standard for the determination of the fluorescence quantum yields.

Viscosity Measurements. The viscosities of the surfactant solutions were measured by using a Fungilab Expert L viscometer. The sample temperature was maintained constant by a glass-jacked beaker connected to a thermostatic bath. The viscosity measurements were obtained using a spindle attachment. Viscosity values are the average of three distinct measurements.

pH Measurements. The pH measurements were performed at room temperature by using an Orion SA 720 pH-meter equipped with a Metrohm AG 9101 Herisau combined glass electrode.

Determination of the Activity of the Artificial Gland Model. For the implementation of the artificial gland model, a specific weighted amount of the **pDoAO** gel (read paragraph I.3 for the details) was enclosed in a glass tube (having a diameter of 2.20 cm) closed at the bottom by the **DM** adhering to the external glass wall through a rubber band (see Figure 4). This device was maintained within a beaker containing 20 mL of deionized water, thermostated at 298 K, and under constant magnetic stirring (see Figure 4B). The **DM**, conditioned in water about 15 h before investigating the behavior of the artificial gland model, was wholly dipped in water. Specific amounts of the CH_3SO_3H and NaOH solutions were injected from the top of the glass tube to induce the gel-to-sol and the sol-to-gel transitions, respectively. To monitor the activity of the artificial gland model, we selected **C_8Ac** as a fluorescent probe. At regular time intervals, the absorption and emission spectra of 2 mL taken from the 20 mL water solution, collecting the molecules released by the artificial gland model, were recorded. The absorption spectra were useful to determine the amount of **pDoAO** molecules lost by the gland. The emission spectra were useful to calculate the amount of **C_8Ac** secreted by the gland. After 5 min, time required to record the absorption and emission spectra, the 2 mL of water, used for the spectrophotometric analysis, was reintroduced within the collecting aqueous solution contained in the beaker. The quantitative determination of the secretory action of **pDoAO** in both the gel and the sol phase was reproduced at least twice.

■ ASSOCIATED CONTENT

Supporting Information

The Supporting Information is available free of charge on the ACS Publications website at DOI: 10.1021/acsomega.8b02940.

Determination of association constants of **ARS** to **pDoAO** micelles; relation between Φ_F(**PyI**) and η; effect of acid and base injections in η of **pDoAO** viscoelastic fluids; activity of the artificial gland; and behavior of the **DM** (PDF)

■ AUTHOR INFORMATION

Corresponding Author

*E-mail: pierluigi.gentili@unipg.it (P.L.G.).

ORCID

Pier Luigi Gentili: 0000-0003-1092-9190

Notes

The authors declare no competing financial interest.

■ ACKNOWLEDGMENTS

Authors acknowledge the financial support by the University of Perugia (Fondo Ricerca di Base 2014, D. D. n. 170, 23/12/2014). N.E.C.-R. thanks the American Chemical Society IREU Program and the National Science Foundation for support under award number DMR-1262908. The authors thank Prof. C. Fortuna of the University of Catania for the synthesis of **PyI**.

■ REFERENCES

(1) Russell, S. J.; Norvig, P. *Artificial Intelligence-A Modern Approach*, 3rd ed.; Pearson Education Limited: Essex, U.K., 2016.

(2) Hagiya, M.; Konagaya, A.; Kobayashi, S.; Saito, H.; Murata, S. Molecular robots with sensors and intelligence. *Acc. Chem. Res.* **2014**, *47*, 1681−1690.

(3) Otero, T. F.; Martinez, J. G.; Arias-Pardilla, J. Biomimetic electrochemistry from conducting polymers. A review. *Electrochim. Acta* **2012**, *84*, 112−128.

(4) Hu, C.; Pané, S.; Nelson, B. J. Soft Micro- and Nanorobotics. *Annu. Rev. Contr. Robot. Autonom. Syst.* **2018**, *1*, 53−75.

(5) Grančič, P.; Štěpánek, F. "Chemical swarm robots". In *Handbook of Collective Robotics—Fundamentals and Challenges*; Kernbach, S., Ed.; Pan Stanford Publishing: Singapore, 2011.

(6) Hu, W.; Lum, G. Z.; Mastrangeli, M.; Sitti, M. Small-scale soft-bodied robot with multimodal locomotion. *Nature* **2018**, *554*, 81−85.

(7) Adamatzky, A.; de Lacy Costello, B.; Melhuish, C.; Ratcliffe, N. Experimental implementation of mobile robot taxis with onboard Belousov-Zhabotinsky chemical medium. *Mater. Sci. Eng., C* **2004**, *24*, 541−548.

(8) Hess, H.; Ross, J. L. Non-equilibrium assembly of microtubules: from molecules to autonomous chemical robots. *Chem. Soc. Rev.* **2017**, *46*, 5570−5587.

(9) Lund, K.; Manzo, A. J.; Dabby, N.; Michelotti, N.; Johnson-Buck, A.; Nangreave, J.; Taylor, S.; Pei, R.; Stojanovic, M. N.; Walter, N. G.; Winfree, E.; Yan, H. Molecular robots guided by prescriptive landscapes. *Nature* **2010**, *465*, 206−210.

(10) Kassem, S.; Lee, A. T. L.; Leigh, D. A.; Markevicius, A.; Solà, J. Pick-up, transport and release of a molecular cargo using a small-molecule robotic arm. *Nat. Chem.* **2015**, *8*, 138−143.

(11) Tregubov, A. A.; Nikitin, P. I.; Nikitin, M. P. Advanced Smart Nanomaterials with Integrated Logic-Gating and Biocomputing: Dawn of Theranostic Nanorobots. *Chem. Rev.* **2018**, *118*, 10294−10348.

(12) Gentili, P. L.; Rightler, A. L.; Heron, B. M.; Gabbutt, C. D. Extending human perception of electromagnetic radiation to the UV region through biologically inspired photochromic fuzzy logic (BIPFUL) systems. *Chem. Commun.* **2016**, *52*, 1474−1477.

(13) Gentili, P. L.; Rightler, A. L.; Heron, B. M.; Gabbutt, C. D. Discriminating between the UV-A, UV-B and UV-C regions by novel Biologically Inspired Photochromic Fuzzy Logic (BIPFUL) systems: A detailed comparative study. *Dyes Pigm.* **2016**, *135*, 169−176.

(14) Gentili, P. L. The fuzziness of a chromogenic spiroxazine. *Dyes Pigm.* **2014**, *110*, 235−248.

(15) Gentili, P. L.; Giubila, M. S.; Germani, R.; Romani, A.; Nicoziani, A.; Spalletti, A.; Heron, B. M. Optical Communication among Oscillatory Reactions and Photo-Excitable Systems: UV and Visible Radiation Can Synchronize Artificial Neuron Models. *Angew. Chem., Int. Ed.* **2017**, *56*, 7535−7540.

(16) Gentili, P. L.; Giubila, M. S.; Germani, R.; Heron, B. M. Photochromic and luminescent compounds as artificial neuron models. *Dyes Pigm.* **2018**, *156*, 149−159.

DOI: 10.1021/acsomega.8b02940
ACS Omega 2018, 3, 16777−16783

(17) Gentili, P. L.; Horvath, V.; Vanag, V. K.; Epstein, I. R. Belousov-Zhabotinsky "Chemical Neuron" as a Binary and Fuzzy Logic Processor. *Int. J. Unconv. Comput.* **2012**, *8*, 177−192.
(18) Brinchi, L.; Germani, R.; Di Profio, P.; Marte, L.; Savelli, G.; Oda, R.; Berti, D. Viscoelastic solutions formed by worm-like micelles of amine oxide surfactant. *J. Colloid Interface Sci.* **2010**, *346*, 100−106.
(19) Goracci, L.; Germani, R.; Rathman, J. F.; Savelli, G. Anomalous behavior of amine oxide surfactants at the air/water interface. *Langmuir* **2007**, *23*, 10525−10532.
(20) Bishop, E. *Indicators*; Pergamon Press: Oxford, 1972.
(21) Carlotti, B.; Cesaretti, A.; Fortuna, C. G.; Spalletti, A.; Elisei, F. Experimental evidence of dual emission in a negatively solvatochromic push-pull pyridinium derivative. *Phys. Chem. Chem. Phys.* **2015**, *17*, 1877−1882.
(22) Chu, Z.; Dreiss, C. A.; Feng, Y. Smart wormlike micelles. *Chem. Soc. Rev.* **2013**, *42*, 7174−7203.
(23) Ahn, S.-k.; Kasi, R. M.; Kim, S.-C.; Sharma, N.; Zhou, Y. Stimuli-responsive polymer gels. *Soft Matter* **2008**, *4*, 1151−1157.
(24) Qiu, Y.; Park, K. Environment-sensitive hydrogels for drug delivery. *Adv. Drug Deliv. Rev.* **2001**, *53*, 321−339.
(25) Koetting, M. C.; Peters, J. T.; Steichen, S. D.; Peppas, N. A. Stimulus-responsive hydrogels: Theory, modern advances, and applications. *Mater. Sci. Eng., R* **2015**, *93*, 1−49.
(26) García, M. T.; Campos, E.; Ribosa, I. Biodegradability and ecotoxicity of amine oxide based surfactants. *Chemosphere* **2007**, *69*, 1574−1578.
(27) Singh, S. K.; Bajpai, M.; Tyagi, V. K. Amine Oxides: A Review. *J. Oleo Sci.* **2006**, *55*, 99−119.
(28) Goracci, L.; Germani, R.; Savelli, G.; Bassani, D. M. Hoechst 33258 as a pH-sensitive probe to study the interaction of amine oxide surfactants with DNA. *ChemBioChem* **2004**, *6*, 197−203.
(29) Yamagishi, A.; Masui, T.; Watanabe, F. Selective activation of reactant molecules by reversed micelles. *J. Phys. Chem.* **1981**, *85*, 281−285.
(30) Burgdorff, C.; Ehrhardt, S.; Loehmannsroeben, H. G. Photophysical properties of tetracene derivatives in solution. 2. Halogenated tetracene derivatives. *J. Phys. Chem.* **1991**, *95*, 4246−4249.

DOI: 10.1021/acsomega.8b02940
ACS Omega 2018, 3, 16777−16783